J. Fluid Mech. (1976), *vol.* 76, *part* 1, *pp.* 157–176
Printed in Great Britain

Precursor shock waves at a slow–fast gas interface

By A. M. ABD-EL-FATTAH, L. F. HENDERSON AND A. LOZZI

Department of Mechanical Engineering, University of Sydney, New South Wales 2006, Australia

(Received 19 December 1975)

This paper presents experimental data obtained for the refraction of a plane shock wave at a carbon dioxide–helium interface. The gases were separated initially by a delicate polymer membrane. Both regular and irregular wave systems were studied, and a feature of the latter system was the appearance of bound and free precursor shocks. Agreement between theory and experiment is good for regular systems, but for irregular ones it is sometimes necessary to take into account the effect of the membrane inertia to obtain good agreement. The basis for the analysis of irregular systems is one-dimensional piston theory and Snell's law.

1. Introduction

A shock wave propagating in any medium will be refracted whenever it encounters a change in the impedance of the medium; a formal definition of this quantity has been given previously (Henderson 1970). It is convenient to think of the refracting wave as passing from an initial medium where it is considered to be the incident shock i to a final medium where it is the transmitted shock t; in addition there will be waves reflected back into the initial medium, which can be either shocks r or expansions e. When all the waves are locally straight and meet at a single point on the impedance interface the refraction is said to be regular, otherwise it is irregular (Taub 1947; Polachek & Seeger 1951; Jahn 1956; Henderson 1966). For some irregular systems t is found to move along the interface at a velocity greater than that of i, and t is then called a *free* precursor shock. However if t propagates at the same velocity as i but with part of it always ahead of i, then t is called a *bound* precursor shock. A necessary condition for the existence of free precursors is that the speed of sound a_i in the initial medium should be less than that in the final medium, a_t, and this is called a slow–fast interface, $a_i < a_t$. A carbon dioxide–helium interface has this property to a marked extent because $a_{CO_2} < a_{He}$ with $a_{He}/a_{CO_2} \approx 3{\cdot}75$. The main objectives of our work were to study the properties of the precursors and the way they were generated. We applied a one-dimensional piston theory to the results and were able to calculate the properties of these waves with good accuracy. For instance, we could calculate the velocity of a free precursor along the interface given only the velocity of the incident shock and the speeds of sound and ratios of specific heats $\gamma_{i,t}$ of the media.

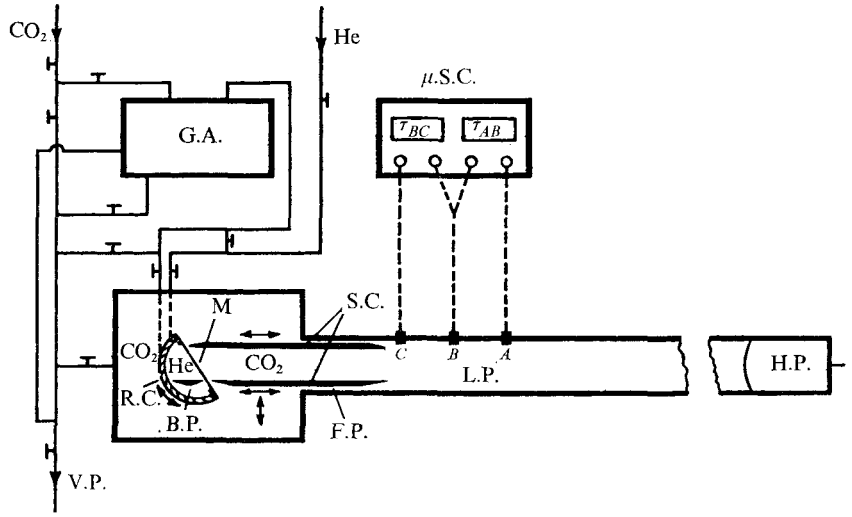

FIGURE 1. Layout of apparatus. G.A., thermal-conductivity gas analyser; μ.S.C., micro-second counter; S.C., shock cutter; M, membrane–interface; L.P., low pressure driver section, CO_2; H.P., high pressure driving section with air as driver gas; V.P., vacuum pump; B.P., back plate; F.P., front plate.

While the theory of regular refraction has been extensively developed by the authors cited above, one difficulty still remains, namely that it nearly always gives multi-valued solutions. This problem has been attacked recently by Henderson & Atkinson (1976), who investigated the stability of each solution by a linearized perturbation of the equations of motion of the flow. One of the interesting properties of the theory for a carbon dioxide–helium interface is that the multi-valued solutions are of an unusual kind, for under certain conditions two solutions with reflected expansion waves are obtained. To the best of our knowledge, no experimental data exist for comparison with a solution set of this type. A secondary objective of our work was to obtain some data for it.

2. Apparatus

The experiments were performed in a conventional shock tube with air as the driver. The layout of the apparatus is shown in figure 1, and some of the details in figure 2. The carbon dioxide and the helium were kept apart by a delicate lacquer membrane; this technique had been used previously by Bitondo (1950), Jahn (1956) and others, but our apparatus was most like that of Jahn. We attempted to refine his equipment in order to use gases with as disparate physical properties as possible, in particular CO_2 and He, instead of air and CH_4, which he had used. It was important for the mass of the membrane to be as small as practicable in order to minimize the effect of its inertia on the wave phenomena. Like Jahn's, our best efforts were centred on the membranes. He mounted them on wire frames which fitted into slots cut in the shock-tube windows. We decided that slots obscured the interface region excessively and decided to do without them. Instead we stretched two wires of diameter 0·254 mm (0·010 in.), and attached

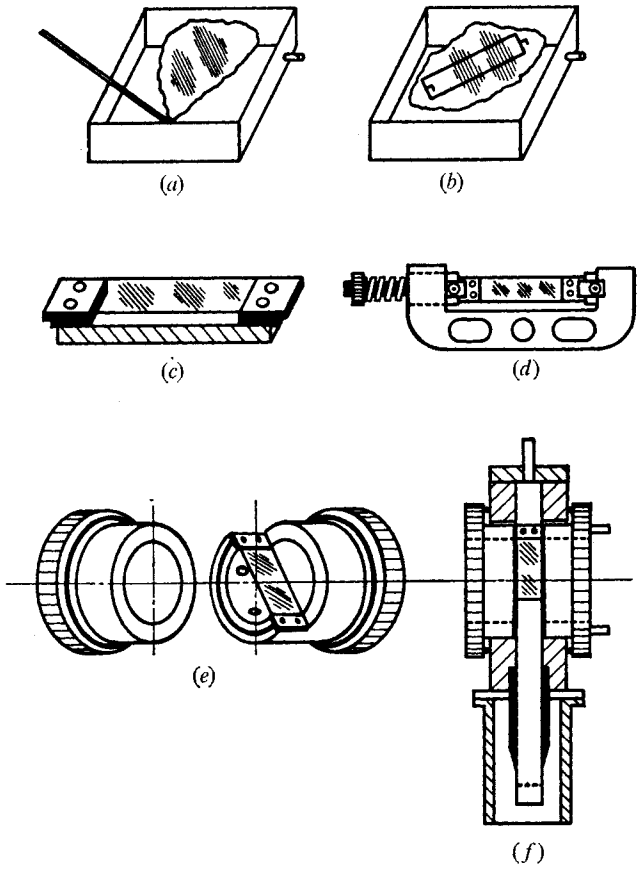

FIGURE 2. Details of membrane preparation. (*a*) Casting. (*b*) Lifting. (*c*) Wire frame and holding plate assembly. (*d*) G-clamp assembly. (*e*) Shock-tube window-frame assembly. (*f*) Plan view of shock-tube working section with refraction cell in position.

them with epoxy resin to two solid mounting blocks (figure 2). A holding plate maintained the frame assembly under tension while it was outside the shock tube. The wires butted directly against the windows, and we relied on the membrane and on a minute amount of silicone grease to effect a seal.

A membrane was prepared by 'casting' it on the surface of filtered water contained in a rectangular tank 76 × 16 cm and about 12½ cm deep. A solution of a commercial vinyl resin (Union Carbide VYNS, copolymer vinyl chloride–vinyl acetate) was prepared in cyclohexanone. A small strip of plastic was dipped into the water and a few drops of the solution were allowed to run from a pipette down the plastic and onto the surface. There they spread out rapidly into a thin film and the membrane formed as the solvent evaporated. It was lifted by an auxiliary frame and transferred to the actual frame which was to be installed in the shock tube. The process was facilitated by a specially made G-clamp, which was so organized that the wires could always be kept under tension while the holding plate was being removed and the frame was being screwed down in the shock tube. The final size of the membrane was 10·01 × 2·54 cm. We measured the thickness of

several samples of it using a Taylor step stylus (Rank Taylor–Hobson), and it varied between 5·5 and 6·5 $\times 10^{-6}$ cm, that is, it was of the order of only 10 molecules thick. The masses of several samples were measured with a microbalance and they varied between 0·5 and 1·0 $\times 10^{-5}$ g cm^{-2}. Measurements of thickness and mass were difficult to make and the accuracy was only good to about two significant figures. The specific gravity obtained from them was about 0·9, compared with the handbook value of 1·35 (Roff 1956, p. 181). Presumably the reduction was due to the evaporation of the solvent creating a somewhat porous structure.

Having installed the membrane, the next task was to introduce carbon dioxide on one side of it and helium on the other, without breaking it, of course. This was done by using the membrane itself as a null-point pressure gauge and with needle valves to induce very slow flow of the gases. The carbon dioxide, being the initial medium, was placed next to the shock-tube diaphragm, and the helium, being the final medium, in a small semicircular cell. The angle of incidence ω_i of the shock i onto the membrane could be varied by rotating the cell. Gas leakage across the membrane was monitored by a thermal conductivity gas analyser (Gow–Mac) which was calibrated by a mixing pump (H. Wörsthoff).

A 'shock cutter' was used in order to present the shock as cleanly as possible to the membrane (figures 1 and 2); it sliced a rectangle from the shock as it passed along the driver section. The position of the cutter could be adjusted to take account of variations in the angle of incidence, and following Jahn we called its bottom plate the front plate. Another movable plate, called the back plate, was placed in the helium cell to try a variety of boundary conditions for the transmitted shock t. The angular positions of these boundaries in relation to the membrane were measured with the help of a cathetometer (Ealing Scientific), accurate to 10′ of arc. The velocity V_i of the incident shock was measured with three lead zirconate titanate transducers (Atlantic Research Corp.) based on the ferro-electric effect.

In our work it was essential to measure the wave angles of the various shocks, expansions, loci and so on which appeared in the refraction. The most accurate method available to us was to use a schlieren (Zeiss) apparatus; its light source was a $\frac{1}{2}\,\mu$s spark stabilized with an argon jet. Angles were measured from schlieren photographs after enlarging them by a factor of about 10 on a profile projector (Nikon); this instrument could measure to about 1′ of arc. However the resolving power of our apparatus and photographs did not permit us to measure to this accuracy: our best measurements were to about 6′.

The sensitivity properties of the transducers made it convenient to do the experiments at a constant velocity V_i of the incident shock. This meant that the Mach number M_{si} normal to i was constant, and also the pressure ratio P/P_1 across it; $P/P_1 \equiv \eta_i = \eta_i(M_{si}, \gamma_1)$. Most experiments were done with $\eta_i = 2$, which corresponds to $V_i = 381$ m s^{-1}, and with ω_i varying from an initially small angle where the refraction was regular to a steadily increasing angle where it became irregular. This procedure was equivalent to starting with a comparatively large free-stream Mach number $M_i = M_{si}/\sin\omega_i$ and ending with a smaller one.

There was a problem with the gases leaking across the membrane; we were able

to reduce this by using double and occasionally triple membranes. As a result the gas analyser showed that the helium was about 90 % pure (10 % by volume carbon dioxide) and the carbon dioxide was about 95 % pure (5 % by volume helium). Owing to the disparity in the molecular weights, namely 4 for helium and 44 for carbon dioxide, contamination of the helium by, say, 5 % of carbon dioxide had a much larger effect on the gas properties (a, γ) than contamination of the carbon dioxide by a similar volume of helium. It is worth noting that the carbon dioxide occupied a considerably larger volume of the shock tube than the helium did, $\approx 250:1$. There was a lapse of about 30 min between setting up the gas interface and firing the shock tube. This was to allow as much time as possible for conditions to become independent of time.

3. Regular refraction

The polar diagrams for refraction at a carbon dioxide–helium interface have an interesting sequence of solution sets. Some of the diagrams we computed for the pure gases are shown in figure 3 and some for the contaminated gases in figure 4. Beginning with ω_i as a small angle, the solution set can be written as

$$RR_1 \equiv \{\epsilon_1, \alpha_1, \alpha_2\},$$

where ϵ_1 represents a regular refraction with a reflected expansion e, and is the solution with smallest entropy production $\dot{S}$, while α_1 and α_2 represent regular refractions with reflected shocks r, and have successively larger $\dot{S}$. If ω_i is now gradually increased the transition condition $\alpha_1 \equiv \alpha_2 \equiv \epsilon_2$ is eventually attained, where ϵ_2 represents another solution with a reflected expansion. With any further increase in ω_i we get $RR_2 \equiv \{\epsilon_1, \epsilon_2\}$, and as the process continues, a second transition is reached: $\epsilon_1 \equiv \epsilon_2$. Beyond this point the solution set is empty, and the refraction must therefore become irregular. A similar sequence has been discussed in detail previously (Henderson 1967).

Using the method described by Henderson (1966) we calculated numerical values for regular refraction for the uncontaminated carbon dioxide–helium interface; these are shown in figures 5 and 6, and some results for the transition conditions are shown in figure 7. We also calculated the effect of variation in the specific heats of carbon dioxide, and the result is shown for the $\eta_i = 6$ case in figure 6. In addition, for comparison with the experimental data we calculated the wave angles at the contaminated interface, taking 90 % purity for helium and 95 % for carbon dioxide. These last data are presented in figure 8, along with the corresponding experimental data. We conclude that it is the ϵ_1 (minimum $\dot{S}$) solution which agrees with experiment and that it does so within the limits of experimental error, while the ϵ_2 solution does not agree. The polar diagrams (figures 3 and 4) show that ϵ_1 has supersonic flow downstream of t and e for most of the range of ω_i for which it exists, and therefore according to the linearized stability theory of Henderson & Atkinson it should be stable. On the other hand ϵ_2 always has subsonic flow downstream of t and therefore should be unstable. A schlieren photograph of a typical ϵ_1-type regular refraction is shown in figure 9 (plate 1); in this particular case the back plate is in line with the front plate.

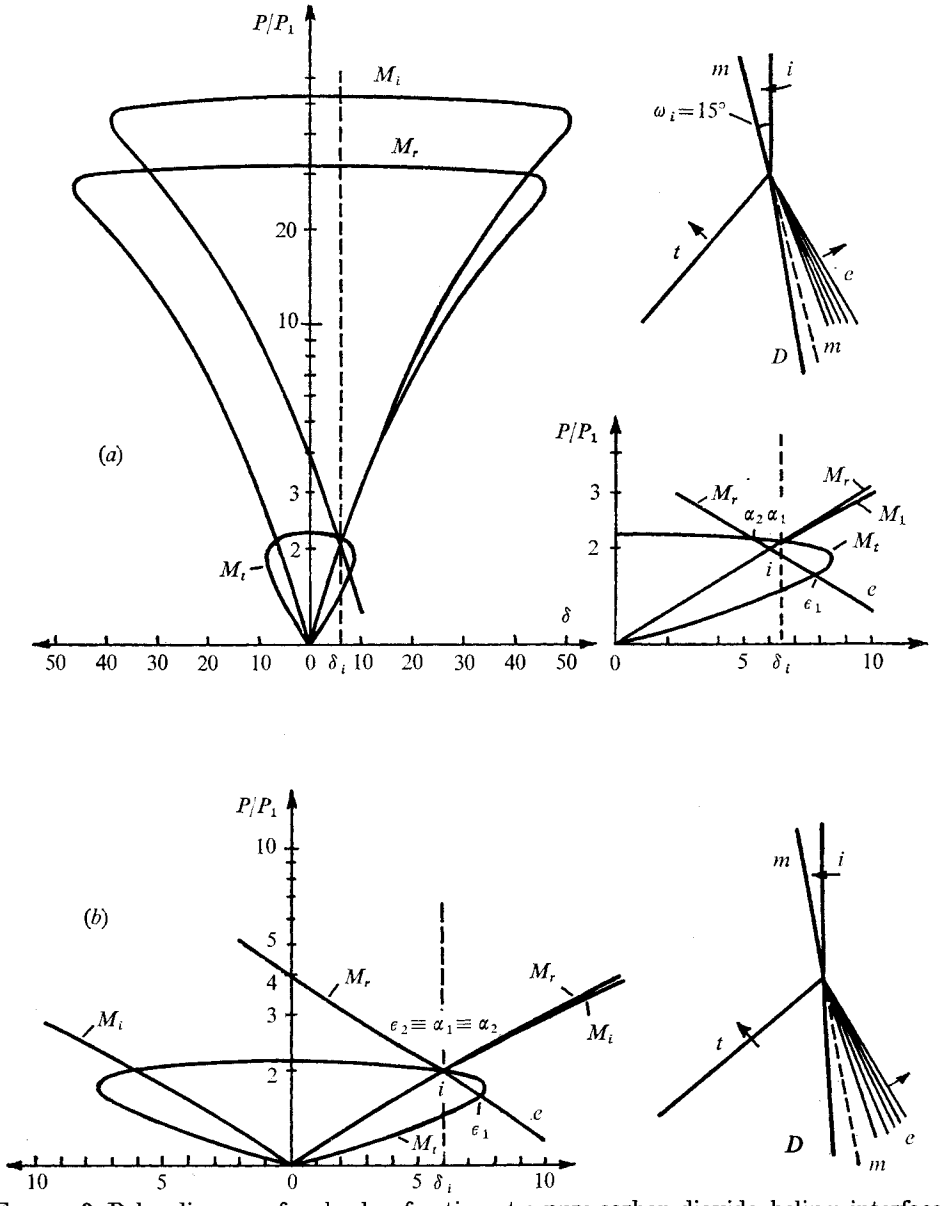

FIGURE 3. Polar diagrams for shock refraction at a pure carbon dioxide–helium interface. (*a*) Regular-refraction solution set $RR_1 \equiv \{\epsilon_1, \alpha_1, \alpha_2\}$ at $\omega_i = 15{\cdot}00°$. (*b*) First-transition condition $\epsilon_2 \equiv \alpha_1 \equiv \alpha_2$ at $\omega_i = 15{\cdot}36°$. (*c*) Regular-refraction solution set $RR_2 \equiv \{\epsilon_1, \epsilon_2\}$ at $\omega_i = 15{\cdot}46°$. (*d*) Second-transition condition $\epsilon_1 \equiv \epsilon_2$ at $\omega_i = 15{\cdot}56°$. (*e*) The regular-refraction solution set is empty at $\omega_i \equiv 16{\cdot}00°$, and the refraction is irregular. *i*, incident shock; *t*, transmitted shock; *e*, reflected expansion; *mm*, position of undisturbed membrane–interface; *D*, deflected interface; *P*, pressure; δ, streamline deflexion; *M*, Mach number.

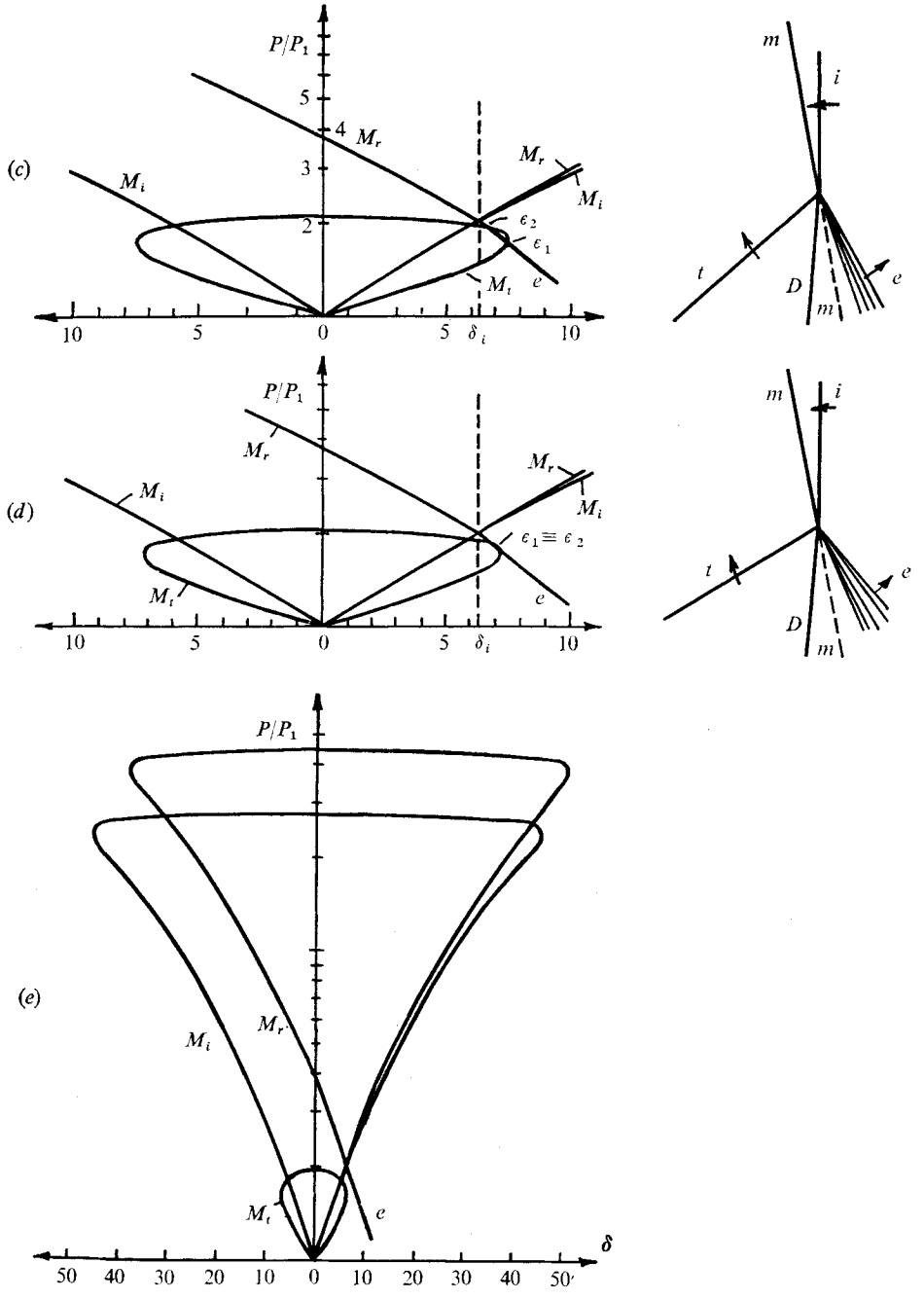

FIGURES 3 (*c–e*). For caption see facing page.

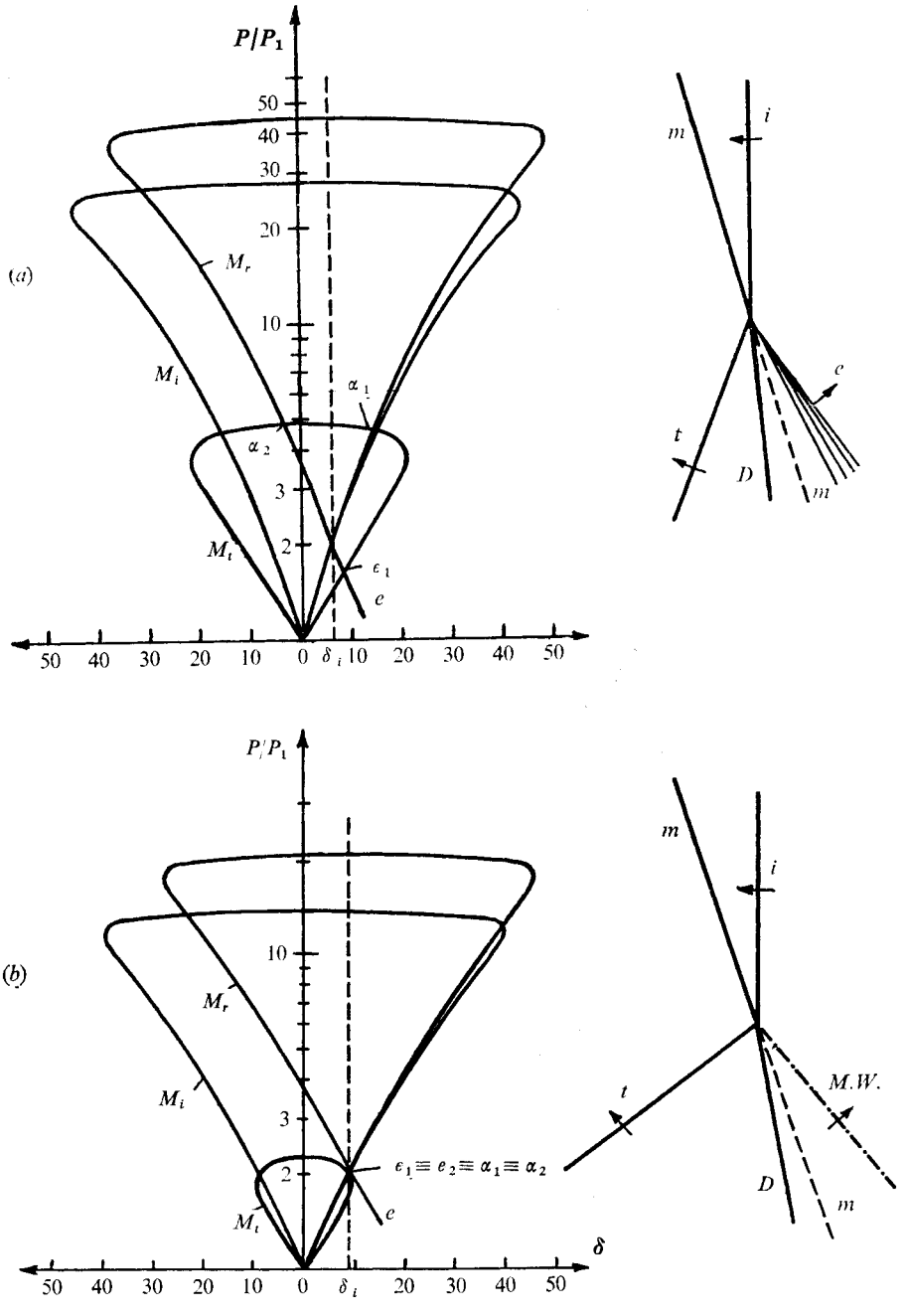

FIGURE 4. Polar diagrams for shock refraction at a contaminated carbon dioxide–helium interface. (*a*) Regular-refraction solution set $RR_1 \equiv \{\epsilon_1, \alpha_1, \alpha_2\}$ at $\omega_i = 16{\cdot}00°$. (*b*) Transition condition $\epsilon_1 \equiv \epsilon_2 \equiv \alpha_1 \equiv \alpha_2$ at $\omega_i = 23{\cdot}12°$. *M.W.*, Mach wave. For symbols see caption to figure 3.

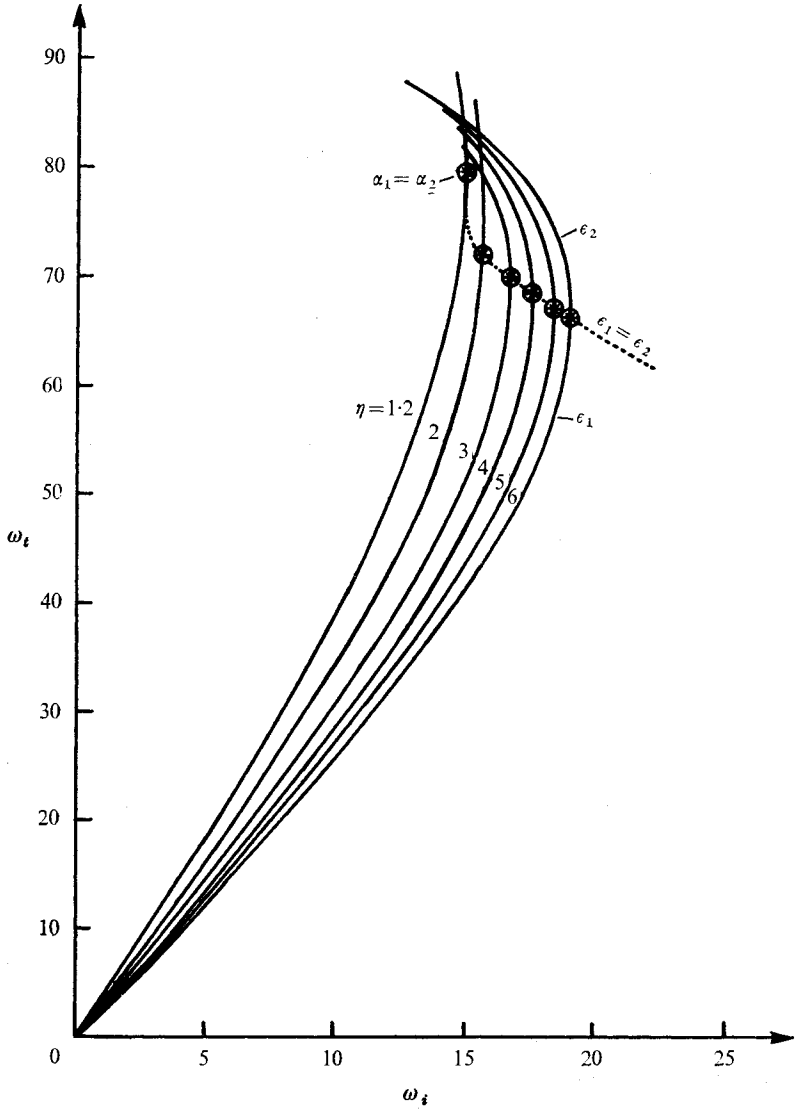

FIGURE 5. Angle of refraction ω_t *vs.* angle of incidence ω_i for the refraction of a plane shock at a pure carbon dioxide–helium interface.

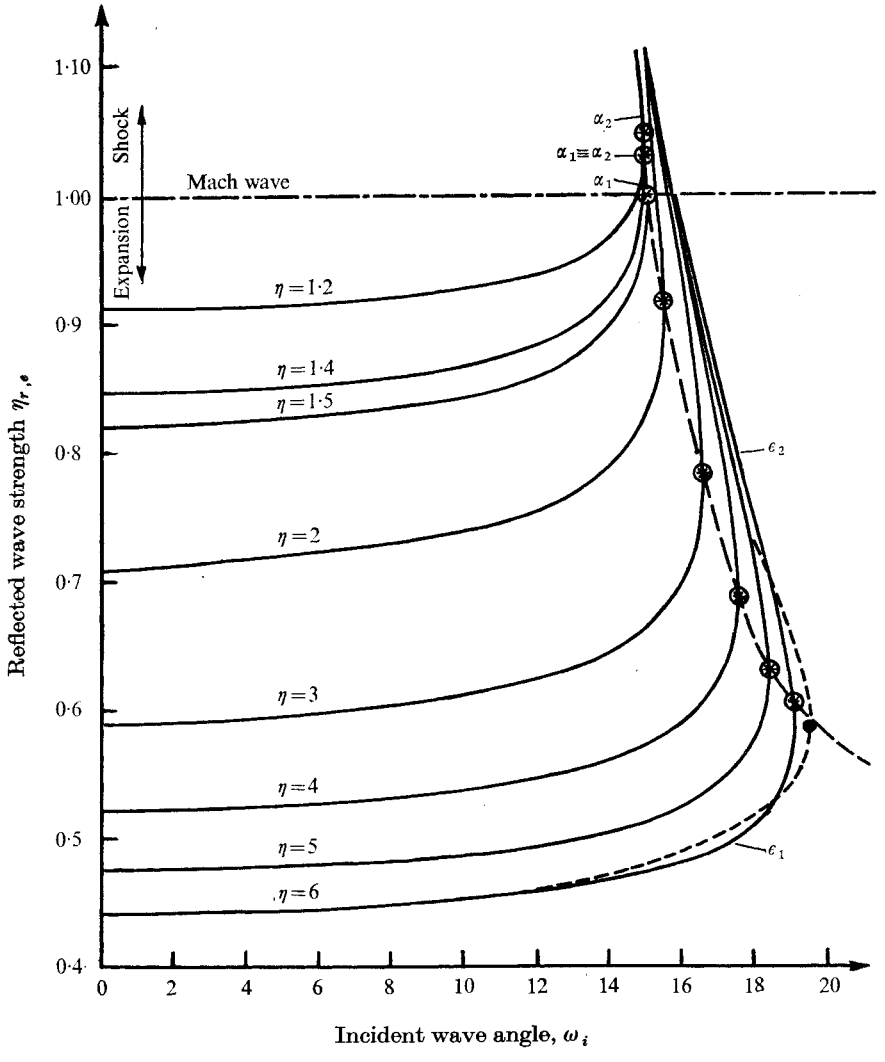

FIGURE 6. Pressure ratio $\eta_{r,e}$ of reflected wave e or r *vs.* angle of incidence ω_i for the refraction of a plane shock at a pure carbon dioxide–helium interface. – – – –, imperfect gas correction, due to variation in specific heats of carbon dioxide for $\eta = 6$; ——, limit of regular refraction.

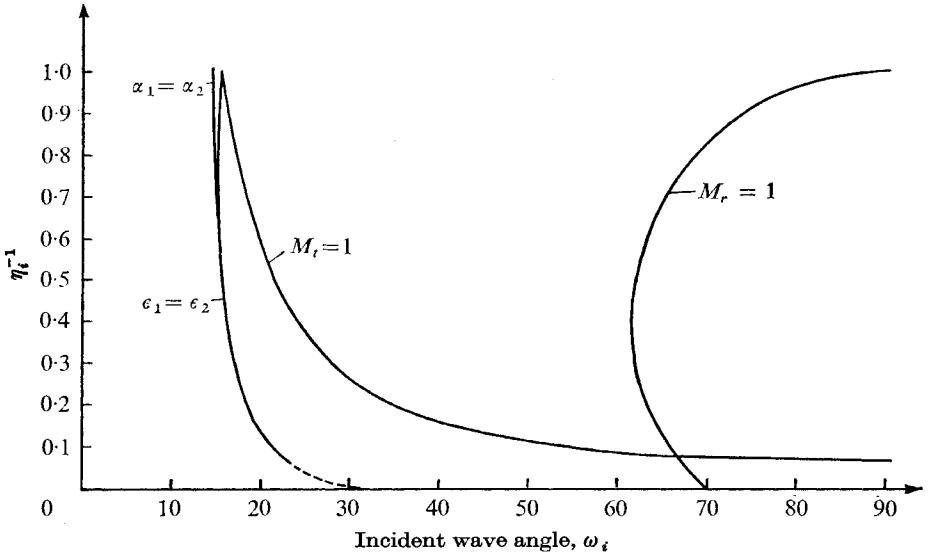

FIGURE 7. Transition and other limiting angles for refraction of a plane shock at a pure carbon dioxide–helium interface.

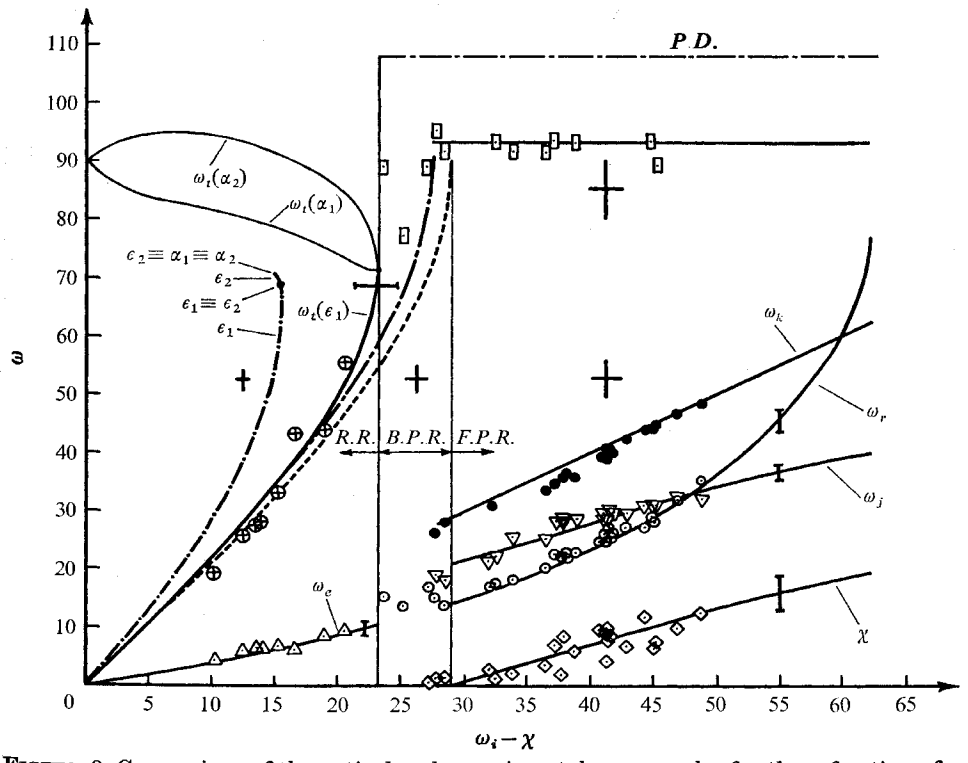

FIGURE 8. Comparison of theoretical and experimental wave angles for the refraction of a plane shock at a contaminated carbon dioxide–helium interface. *R.R.*, regular refraction; *B.P.R.*, bound-precursor irregular refraction; *F.P.R.*, free-precursor irregular refraction; – – – –, Snell–piston theory; —·—·—, piston–diaphragm theory applied to regular refraction with $\omega_i = 0$; *P.D.*, piston–diaphragm theory applied to free-precursor shocks; +, size of experimental error; $\overline{\mathrm{I}}$, effect of ± 2 % change in gas contamination. For other symbols see captions to figures 3, 9 and 10.

4. Irregular refraction

4.1. *Experimental data*

A typical irregular wave system is shown in figure 10 (plate 2). Perhaps its most striking feature is that t has moved ahead of i to become a precursor shock, and that t has in its turn transmitted a new shock j back into the carbon dioxide. The j wave, which is itself a precursor, interacts with the oncoming i shock at the point X and alters it; the modified i shock has been labelled k. When k reaches the interface it reflects as an expansion wave e, and this local interaction can be regarded as total internal reflexion. Wave systems similar to the one shown in figure 10 have also been photographed at an air–methane interface by Jahn using an interferometer, and they are known in acoustics, where the j precursor is sometimes called the *lateral* wave (Landau & Lifshitz 1959, p. 273).

In figure 10 the back plate is again in line with the front plate and t is found to be very nearly a portion of a cylinder centred on the corner formed by the interface and the plates. We studied the radial velocity of t in a series of seven experiments in which $\omega_i = 50°$, $V_i = 381\ \mathrm{m\ s^{-1}}$ and indeed all the parameters were held constant: we merely varied the time delay in photographing the wave system so as to find out how it developed in time τ. The results are plotted in the x, τ plane in figure 11. The velocities are given by the slopes of the lines; $V_i = 381\ \mathrm{m\ s^{-1}}$ (or $V = 381/\sin 50° = 497\ \mathrm{m\ s^{-1}}$ along the interface) is of course constant because we imposed this as a constraint, but it will be seen that $V_t = 787\ \mathrm{m\ s^{-1}}$ is also constant, and that $V_t > V_i$. We conclude that t is a *free* precursor, and that its law of propagation is given by

$$V_t = R/\tau = \text{constant}, \tag{1}$$

where R is the shock radius. It follows that the motion of t is self-similar or pseudo-stationary. At first it may seem remarkable that a cylindrical shock can propagate without the slightest sign of decay, but the limit of self-similarity will be reached either when the reflected shock r has swept the full length of i, or when t reaches the end of the back plate, whichever happens sooner. The fact that t is part of a cylinder suggests that its radial velocity is independent of ω_i, at least for the free precursor wave system, and this idea is supported by additional data obtained for other ω_i and plotted in figure 11. We also found that V_t was practically independent of the angular position of the back plate for this wave system and some of these data have been plotted as well.

Self-similar wave systems have been discussed by Jones, Martin & Thornhill (1951), Sternberg (1959) and others. The Jones *et al.* paper shows how the gas motion can be considered as a combination of source and sink flows. For example, taking shock-wave co-ordinates for the system in figure 10, we can think of the supersonic flow approaching i as coming from a source at infinity and flowing radially towards a sink at the corner. The local wave angle at any point on i is measured from the straight line joining the point to the corner, and in particular the maximum value of this angle ω_i will be at the point X. It is easy to measure the angle χ between the interface and the straight line joining X to the corner (the trajectory path of X), and some results of doing so are shown in figure 8. We

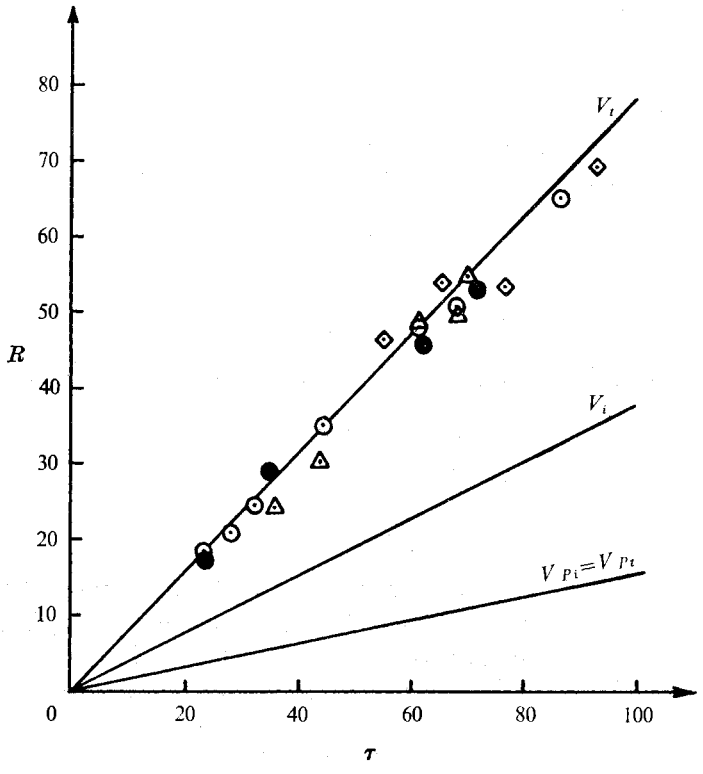

FIGURE 11. Comparison of theoretical and experimental wave velocity diagrams for free-precursor irregular refraction. V_t, free-precursor transmitted shock velocity; $V_i = 381\,\mathrm{m\,s^{-1}}$, incident shock velocity; V_{Pi}, $V_{Pt} = 154\,\mathrm{m\,s^{-1}}$, piston velocity of incident and transmitted shocks respectively; ——, $V_t = 787\,\mathrm{m\,s^{-1}}$, calculated from piston theory; ⊙, *B.P.* in line with *F.P.*, $\omega_t = 50°$; ◇, *B.P.* in line with *F.P.*, $\omega_t \neq 50°$; ●, *B.P.* not in line with *F.P.*, but at other angular positions relative to *F.P.*; △, *B.P.* parallel to undisturbed interface; τ, time; *R*, shock radius.

see that X propagates in a straight line, which is as it should be if system is self-similar. We measured in addition the wave angles of j, k and r at X and the results are also shown in figure 8.

4.2. *Piston theory of the t precursor*

Consider the one-dimensional motion of a plane piston starting impulsively with a finite velocity V_p and driving into a perfect gas initially at rest. A shock with a velocity V_w, say, will therefore be generated, and it will be assumed that all of the gas between the piston and the shock will be uniformly compressed. Then, by conservation of mass, for a piston of unit cross-section, we have (Zeldovich & Raizer 1966, pp. 45–47)

$$\frac{\rho}{\rho_1} = \frac{V_w \tau}{V_w \tau - V_p \tau} = \frac{V_w}{V_w - V_p}, \tag{2}$$

while from conservation of momentum

$$P - P_1 = \rho_1 V_w V_p \tag{3}$$

and from conservation of energy

$$PV_p = \rho_1 V_w[C_v(T-T_1)+\tfrac{1}{2}V_p^2], \tag{4}$$

for density ρ, pressure p, temperature T and specific heat at constant volume C_v. A subscript 1 refers to the undisturbed gas, and the absence of a subscript to the disturbed gas. Using the equation of state $P = \rho RT$, and the fact that

$$C_v = R/(\gamma-1),$$

(4) becomes

$$PV_p = \rho_1 V_w\left[\frac{1}{(\gamma-1)}\left(\frac{P}{\rho}-\frac{P_1}{\rho_1}\right)+\tfrac{1}{2}V_p^2\right]. \tag{5}$$

Eliminating P and ρ by using (2) and (3), we get after a short calculation†

$$V_w^2-\tfrac{1}{2}(\gamma+1)V_pV_w-a_1^2 = 0, \tag{6}$$

or in terms of the piston velocity

$$V_p = \frac{2}{\gamma+1}\frac{V_w^2-a_1^2}{V_w}. \tag{7}$$

In order to apply (6) or (7) to the free precursor t we assume that the piston velocity for i is equal to the velocity of the contact discontinuity between the carbon dioxide and the driving mass of air. Using (7) we find this to be 154 m s^{-1}, but from an examination of several photographs similar to the one shown in figure 10 we also find that the CO_2–He interface has the same velocity as the driving piston. This means that the piston velocities of i and t are equal; we shall make this assumption and return to it at the end of the paper. Then we get from (7)

$$\frac{1}{\gamma_1+1}\frac{V_i^2-a_1^2}{V_i} = \frac{1}{\gamma_4+1}\frac{V_t^2-a_4^2}{V_t}, \tag{8}$$

or

$$V_t = \tfrac{1}{2}[b \pm (b^2+4a_4^2)^{\frac{1}{2}}], \tag{9}$$

where

$$b \equiv \frac{\gamma_4+1}{\gamma_1+1}\frac{V_i^2-a_1^2}{V_i}, \tag{10}$$

and where $a_{1,4}$ are the speeds of sound in the undisturbed carbon dioxide and helium respectively and $\gamma_{1,4}$ are the corresponding specific-heat ratios. The positive root of (9) is taken because it applies to a forward-moving wave. We computed V_t from (9) and (10), and the result is compared with experiment in figure 11. The agreement is within the limits of experimental error, which is gratifying in view of the simplicity of the theory and its assumptions. Equations (9) and (10) are independent of ω_i and so therefore is V_t; we have already noted that the experiments indicate the same conclusion. The pressure ratio across a shock can also be obtained from the piston theory:

$$\frac{p}{p_1} = \frac{2\gamma}{\gamma+1}M_s^2-\frac{\gamma-1}{\gamma+1}, \tag{11}$$

where $M_s = V_w/a_1$ is the shock Mach number.

† We are indebted to Professor G. A. Bird for drawing our attention to this formula.

The law of propagation for the cylindrical precursor shock t can now be stated as

$$V_t = R/\tau = \tfrac{1}{2}[b + (b^2 + 4a_4^2)^{\frac{1}{2}}], \tag{12}$$

which is more general than (1) because it can be applied to a shock propagating into a gas with slowly changing a_4 and γ_4 and with a slowly changing driving shock velocity V_i.

4.3. *Piston–diaphragm theory of the j precursor*

The basis for calculating the velocity V_j of the j precursor is to assume that the membrane behaves like a shock-tube diaphragm. The diaphragm pressure ratio P_4/P_1 (figure 12) will be equal to that across the t shock, and it will be assumed that t ruptures the membrane continuously as it sweeps across it. It follows that not only will j be continuously generated in time, but there must also be an expansion wave generated continuously in time which propagates back into the helium. Now the flow downstream of t is subsonic, so the expansion can instantly overtake t at the interface and weaken it, and therefore perturb it from its cylindrical shape in this region.

In order to calculate the local wave angles of t and j we apply the theory normal to the membrane (figure 12*b*). First, the shock Mach number M_{sj} of the j wave can be found from (Gaydon & Hurle 1963, p. 20)

$$\frac{P_4}{P_1} = \frac{2\gamma_1 M_{sj} - (\gamma_1 - 1)}{\gamma_1 + 1}\left\{1 - \frac{\gamma_4 - 1}{\gamma_1 + 1}\frac{a_1}{a_4}\left(M_{sj} - \frac{1}{M_{sj}}\right)\right\}^{-2\gamma_4/(\gamma_4 - 1)} \tag{13}$$

Next, the free-stream Mach number of j along the interface (M_{ij}) is given by

$$M_{1j} = V_j/a_1 = V_t/a_1, \tag{14}$$

and from (13) and (14) the wave angle $\omega_j - \chi$ which j makes with the interface is given by

$$\omega_j - \chi = \sin^{-1} M_{sj}/M_{1j}. \tag{15}$$

The normal velocity V_2 of the interface after it has been disturbed by t can now be found from (Gaydon & Hurle)

$$V_2 = \frac{2a_1}{\gamma_1 + 1}\left(M_{sj} - \frac{1}{M_{sj}}\right), \tag{16}$$

where V_2 is also simultaneously both the driving-piston velocity of the j wave and the withdrawing-piston velocity of the expansion wave: $V_2 = V_3$. The pressure ratio P_4/P_2 across this last wave is obtained from ($P_3 = P_2$)

$$\frac{P_4}{P_2} = \left(\frac{a_4}{a_4 - \frac{\gamma_4 - 1}{2}V_2}\right)^{2\gamma_4/(\gamma_4 - 1)} = \left\{1 - \frac{\gamma_4 - 1}{\gamma_1 + 1}\frac{a_1}{a_4}\left(M_{sj} - \frac{1}{M_{sj}}\right)\right\}^{-2\gamma_4/(\gamma_4 - 1)}, \tag{17}$$

where we have made use of (16). Comparing (13) and (17) and noting (11), the pressure ratio P_2/P_1 of the perturbed t precursor at the interface is given by

$$\frac{P_2}{P_1} = \frac{P_4}{P_1}\frac{P_2}{P_4}. \tag{18}$$

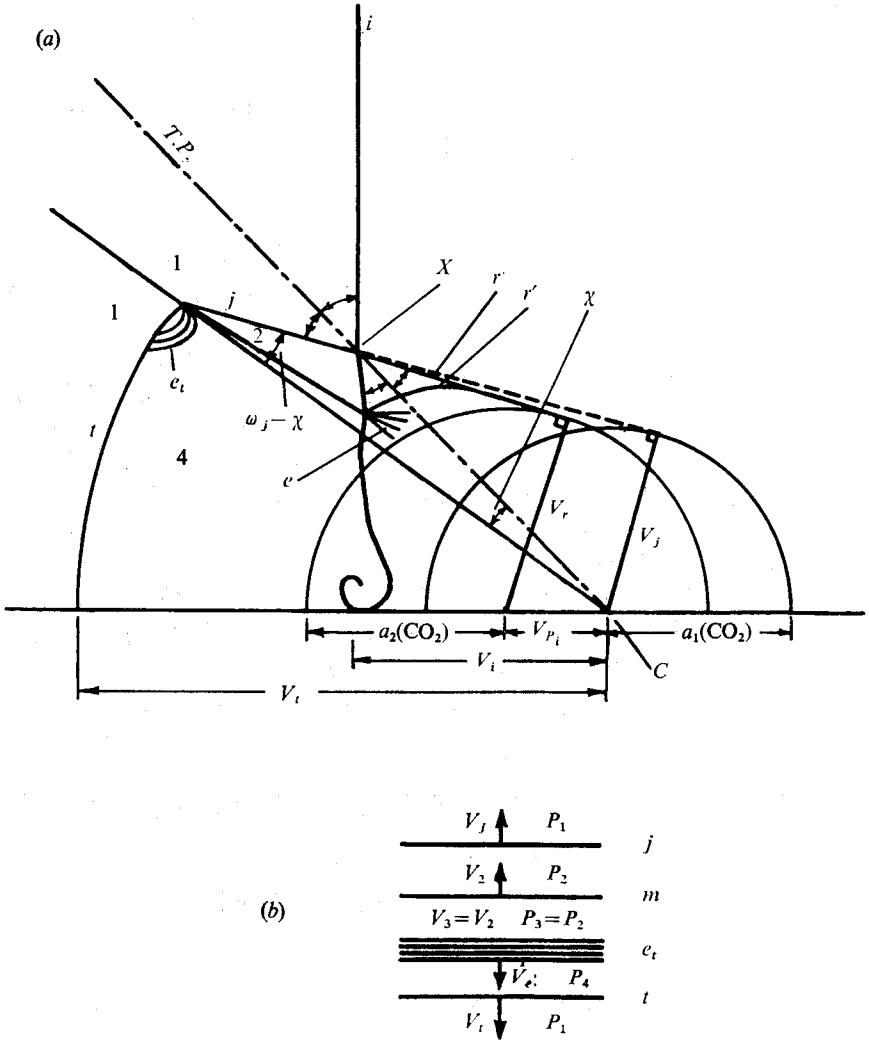

FIGURE 12. Nomenclature for the piston–diaphragm theory. e_t, expansion wave which overtakes t. Note: the waves are shown propagating normal to the membrane–interface in (*b*) but there is a parallel flow superimposed on them. The e_t and t waves are shown separated to facilitate the definition of the subscripts; in reality these two waves are partially or wholly combined, and t is perturbed from its cylindrical shape. For other symbols see captions to figures 3 and 10.

From this last result we can use (11) to calculate the shock Mach number of t at the interface, and then find its local wave angle by using equations analogous to (14) and (15). With this information available it is straightforward to calculate χ from the wave geometry, and then from wave interaction theory to calculate the wave angles of j, k and r at their intersection point X. For this purpose the Huygen construction shown in figure 12 is useful. The j wave proceeds into the undisturbed gas, so its source is located at the corner C, but r propagates into the disturbed gas behind i, so its source must move along the back plate at the piston velocity of i, namely V_{Pi}.

As a result of the calculations, we obtained $\omega_j - \chi = 23{\cdot}0°$, compared with $21{\cdot}5°$ from experiment; the agreement is only fair. However there are large discrepancies for the other wave angles; for example we got $\omega_t = 107{\cdot}6°$ at the interface (t is inclined forward when $\omega_t > 90°$) compared with $93{\cdot}0°$ from experiment (figure 8), and there were also large discrepancies for ω_j, ω_k and ω_r. In seeking an explanation we were led to consider the effect of the membrane inertia.

4.4. *The effect of membrane inertia on the t and j precursors*

Jahn (1954) studied this effect for the special case of the shock colliding head-on with the membrane, and found it to be negligible. Some of our results support this conclusion; for example there is good agreement between theory and experiment for regular refraction, and the piston theory for the radial velocity of t also agrees well with experiment. However t strikes the membrane at almost glancing incidence and a careful study of several photographs seemed to show that it was being deflected intact by t and not being torn into fragments until it encountered the k shock. This observation received further support when it was discovered that there was always a weak shock r' (figure 10) just upstream of the expansion e, which suggested that k was partly reflecting off the membrane, and that it was torn apart an instant after the passage of k. We decided to make a simplified analysis of the inertia effect at glancing incidence.

The membrane is itself a compressible substance, and t must therefore continuously transmit a longitudinal pulse into it. Applying (3) to this wave gives

$$P_3 - P_2 = \rho_m V_m V_{Pm}, \tag{19}$$

where ρ_m is the membrane density, V_m the velocity of the compression wave in it, and V_{Pm} the corresponding piston velocity. Applying (3) also to the perturbed t wave at the interface yields

$$P_3 - P_1 = \rho_h V_t' V_{Pt}, \tag{20}$$

where ρ_h is the undisturbed density of helium, V_t' the velocity of the perturbed t wave at the interface and V_{Pt} the piston velocity. It will be recognized that $\rho_m V_m$ and $\rho_h V_t'$ are the acoustic impedances provided that V_m and V_t' are not too different in magnitude from the respective speeds of sound. Comparing (19) and (20) and remembering that the pressure forces are of the same order of magnitude, we see that the impedances are of different order. In fact, if we assume (Courant & Friedrichs 1948, p. 239) that $V_m \sim (E_m/\rho_m)^{\frac{1}{2}}$, where E_m is Young's modulus for the membrane material, then we find $\rho_m V_m / \rho_h V_t' \sim 10^4$, and therefore

$$V_{Pm}/V_{Pt} \sim 10^{-4}.$$

Now $V_{Pt} \approx 150\,\mathrm{m\,s^{-1}}$, so $V_{Pm} \approx 0{\cdot}015\,\mathrm{m\,s^{-1}}$. Finally, because $V_{Pm} = V_{Pj}$, where V_{Pj} is the piston velocity of j, we see that j is virtually an acoustic compression, i.e. $V_j \approx a_1$ (figure 12). The t precursor adjusts its wave angle at the interface such that the component of its piston velocity normal to the interface is equal to V_{Pm}. From all of this information we were able to calculate χ, and the wave angles of j, k and r at their intersection X. The results are compared with experiment in figure 8, and while there is still some small discrepancy the accuracy of the theory

is greatly improved by taking the membrane inertia into account; in fact the theory now agrees with the data within the limits of experimental error.

When calculating V_m we used the handbook values of E_m from Roff (1956, p. 182) and our measured value of ρ_m. We had no way of measuring E_m for such a very thin film,† but the theory would agree better with experiment if E_m were significantly smaller than the value for the bulk material.

5. Regular–irregular transition, bound precursors

We now consider in more detail how the regular system changes into the irregular system as ω_i is increased. Snell's law turns out to be very important to the discussion; we may derive it very simply by noting that, for any incident–transmitted–reflected wave system, the velocity V of the waves along the interface must be the same if the system is to exist. For the special case of regular refraction this gives

$$\frac{V_i}{\sin\omega_i} = \frac{V_t}{\sin\omega_t} = V = \frac{V_{en}}{\sin\omega_{en}}, \tag{21}$$

where V_{en} and ω_{en} apply to any wave in the expansion fan. Equation (21) is Snell's law and similar expressions can be written down for other wave combinations such as t and j. Equations (9) and (10) can be used for the relation between V_i and V_t. The result will be called the Snell–piston theory and it gives the following relation between ω_i and ω_t:

$$\sin\omega_t = \tfrac{1}{2}\sin\omega_i\left[\frac{\gamma_4+1}{\gamma_1+1}\frac{V_i^2-a_1^2}{V_i^2}+\left(\left(\frac{\gamma_4+1}{\gamma_1+1}\right)^2\left(\frac{V_i^2-a_1^2}{V_i^2}\right)^2+\frac{4a_4^2}{V_i^2}\right)^{\frac{1}{2}}\right]. \tag{22}$$

In the present instance we put $V_t/V_i = 787/381 = 2{\cdot}07$, so it is simplest to use (21) instead of (22); some numerical results are shown in figure 8. The Snell–piston theory agrees quite well with the exact theory for a useful range of $\omega_i \leqslant 15°$ but it becomes increasingly inaccurate as transition is approached. This is because in using (9) and (10) to find V_t we have neglected the effect of the reflected expansion. We can use the exact theory to calculate the initial value of V_t at $\omega_i = 0$, which is $V_t = 826\,\mathrm{m\,s^{-1}}$ (instead of $787\,\mathrm{m\,s^{-1}}$), and the same result can be obtained from the piston–diaphragm theory.‡ If we substitute this exact value into (21), the Snell–piston theory is significantly improved (figure 8). However V_t is not correct at $\omega_i \neq 0$. We find from the exact theory, combined with (21), that it increases all the way to transition, where it becomes $V_t = 918\,\mathrm{m\,s^{-1}}$.

The wave angle ω_t of t also increases rapidly towards transition, because t must satisfy the compatibility conditions on the pressure P and the streamline deflexion δ along the interface downstream of the refraction point. These well-known conditions are

$$\delta_t = \delta_i + \delta_e, \quad \frac{P_t}{P_1} = \frac{P_i}{P_1}\frac{P_e}{P_i}, \tag{23), (24}$$

† It occurred to us later that perhaps this could be done by measuring the natural frequency of vibration of the membrane on a frame.

‡ The value of V_i/V_t obtained from the the exact theory may be regarded as the relative (shock) refractive index of the media, which suggests in view of Snell's law that a regularly refracting shock obeys Fermat's principle.

where the suffixes i, e and t refer respectively to the flow downstream of the i, e and t waves. Regular refraction will be impossible when t is no longer able to satisfy (23) and (24), and figures 3 (*c*)–(*e*) and 4 illustrate the details of the process as the transition point $\epsilon_1 \equiv \epsilon_2$ is surpassed. Alternatively, according to the Henderson–Atkinson stability theory transition may take place slightly sooner by the ϵ_1 solution becoming unstable at the sonic point on the helium polar. Significantly perhaps, this is also the point where upstream-moving disturbances can first reach the refraction point by overtaking the t shock. Unfortunately these two rival criteria are too close together for the matter to be resolved with our experimental data. One of the difficulties here is that ω_t is very sensitive to any change in the system parameters such as ω_i and the gas contamination, and we found it impossible to measure the transition point precisely. But irrespective of which criterion is valid we shall name the point *the first transition.*

We now have from the exact theory that $V_t = 918\,\mathrm{m\,s^{-1}}$ at transition, and from the piston theory (12) that $V_t = 787\,\mathrm{m\,s^{-1}}$ when t is a free precursor. *Therefore, as the wave system passes through the first transition, t must accelerate with* ω_i *until t becomes a free precursor.* To examine the consequences of this statement we find from the exact theory of regular refraction that $\omega_i = 23{\cdot}12°$ at transition. But we can use (21) to calculate the ω_i for which t first becomes a free precursor, for we know that at this condition $V_t/V_i = 787/381 = 2{\cdot}07$, and from the piston–diaphragm theory we have $\omega_t = 93°$ if there is a membrane or $\omega_t = 107{\cdot}6°$ if there is not. Then (21) gives $\omega_i = 28{\cdot}8°$ or $27{\cdot}4°$ respectively, *both of which differ significantly from* $\omega_i = 23{\cdot}12°$ *at first transition.* Again from (21) we find that the velocity V of i along the interface for $23{\cdot}12 < \omega_i < 28{\cdot}8°, 27{\cdot}4°$ is larger than the free-precursor velocity of t, as indeed it is also for regular refraction, and furthermore $V_t = V$ at the end of the range and $V_t > V$ beyond it. *Hence t is a free precursor only for those values of* $\omega_i > 28{\cdot}8°, 27{\cdot}4°$ *for which* $V_t > V$. We shall name $V_t = V$ *the second transition.*

We consider now the nature of the wave system which lies between the first and second transition, or in our case $23{\cdot}12 < \omega_i < 28{\cdot}8°, 27{\cdot}4°$. A schlieren photograph of it is shown in figure 13 (plate 3). Inspection of several such photographs shows that transition has taken place, and that t is everywhere ahead of i, but only slightly so at the interface. Although the experimental data were not conclusive enough for us to be sure, it appeared also that i and t had the same velocity V along the interface, or very nearly so. All of this points to the conclusion that t is a *bound* precursor in this range. Our experiments could not resolve any difference between V_i and V_t in this range. If therefore t is bound, then presumably it managed to get slightly ahead of i during some non-pseudo-stationary process at the corner. The ranges of ω_i for the three phenomena, namely regular refraction, bound-precursor irregular refraction and free-precursor irregular refraction, are shown in figure 8.

Finally we return to the assumption made in § 4.2, that the piston velocities $V_{Pi,t}$ for i and t are equal when t is a free precursor. We now know that, for the regular and the bound-precursor systems, the velocity V of i along the interface is greater than the free-precursor velocity of t, and therefore, by (7), V_{Pt} must also be greater for those systems than for the free-precursor one. *It follows that t must be driven by the motion of i along the interface.* However V_{Pt} declines with ω_i as the

second transition is approached, where $V = V_t$, and it becomes equal to the free-precursor piston velocity at this point (in fact this could be taken as an alternative definition of this point). With any further increase in ω_i, $V < V_t$, which means that t moves along the interface *faster* than i does, that is t has become a free precursor. By experiment we now find that t is driven by the motion of the deflected interface, and we recall from § 4.2 that this is also equal to the piston velocity V_{Pi} of i. But V_{Pi} is independent of ω_i so therefore V_t must also be independent of ω_i for the free-precursor system.

REFERENCES

BITONDO, D. 1950 *Inst. Aerophys., University of Toronto, U.T.I.A. Rep.* no. 7.

COURANT, R. & FRIEDRICHS, K. O. 1948 *Supersonic Flow and Shock Waves.* Interscience.

GAYDON, A. G. & HURLE, I. R. 1963 *The Shock Tube in High Temperature Chemical Physics.* London: Chapman & Hall.

HENDERSON, L. F. 1966 *J. Fluid Mech.* **26**, 607.

HENDERSON, L. F. 1967 *J. Fluid Mech.* **20**, 385.

HENDERSON, L. F. 1970 *J. Fluid Mech.* **40**, 719.

HENDERSON, L. F. & ATKINSON, J. D. 1976 *J. Fluid Mech.* **75**, 751.

JAHN, R. G. 1954 *Princeton University Tech. Rep.* no. II-16.

JAHN, R. G. 1956 *J. Fluid Mech.* **1**, 457.

JONES, D. M., MARTIN, P. M. E. & THORNHILL, C. K. 1951 *Proc. Roy. Soc.* A **209**, 238.

LANDAU, L. D. & LIFSHITZ, E. M. 1959 *Fluid Mechanics.* Pergamon.

POLACHEK, H. & SEEGER, R. J. 1951 *Phys. Rev.* **84**, 922.

ROFF, W. J. 1956 *Fibre, Plastics and Rubbers, a Handbook of Common Polymers.* Butterworths.

STERNBERG, J. 1959 *Phys. Fluids*, **2**, 179.

TAUB, A. H. 1947 *Phys. Rev.* **72**, 51.

ZELDOVICH, YA. B. & RAIZER, YA. P. 1966 *Physics of Shock Waves and High Temperature Hydrodynamic Phenomena.* Academic.

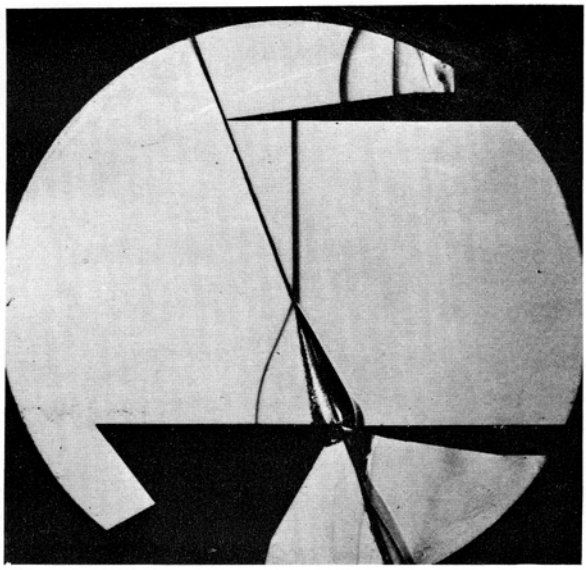

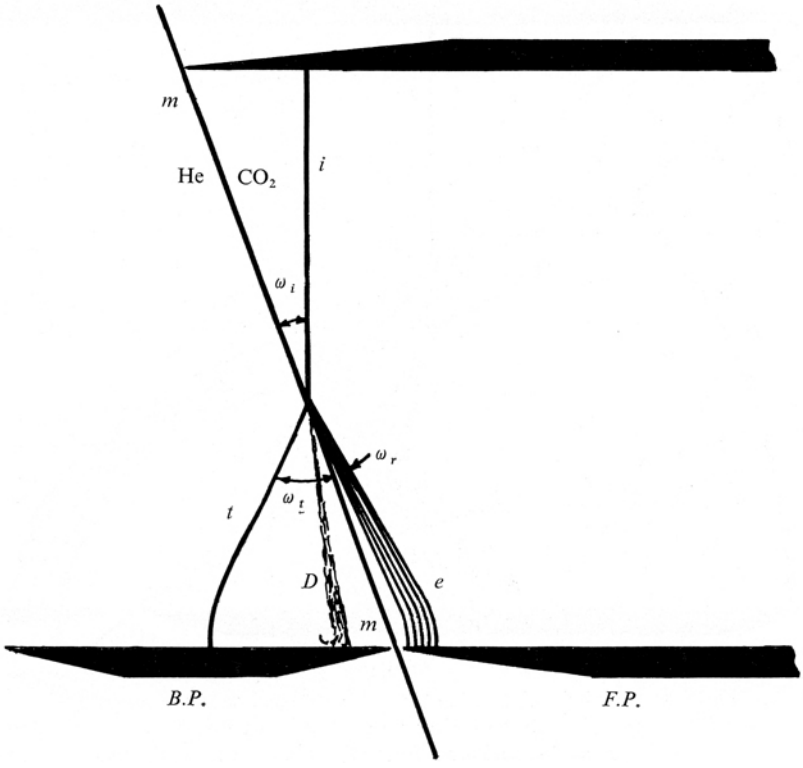

FIGURE 9. Regular refraction of a plane shock at a contaminated carbon dioxide–helium interface. For symbols see caption to figure 3.

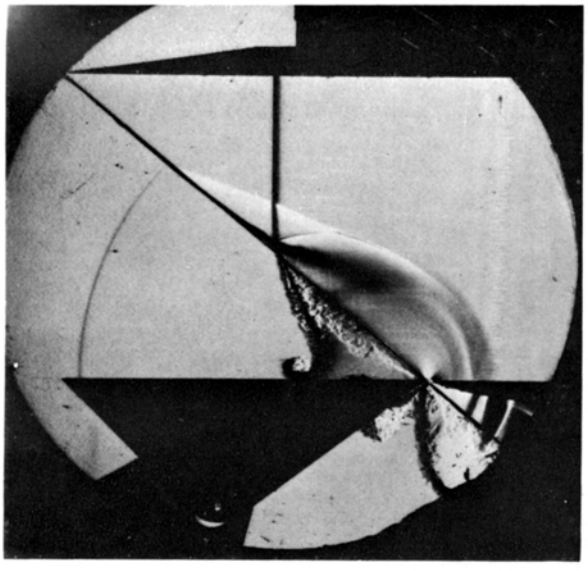

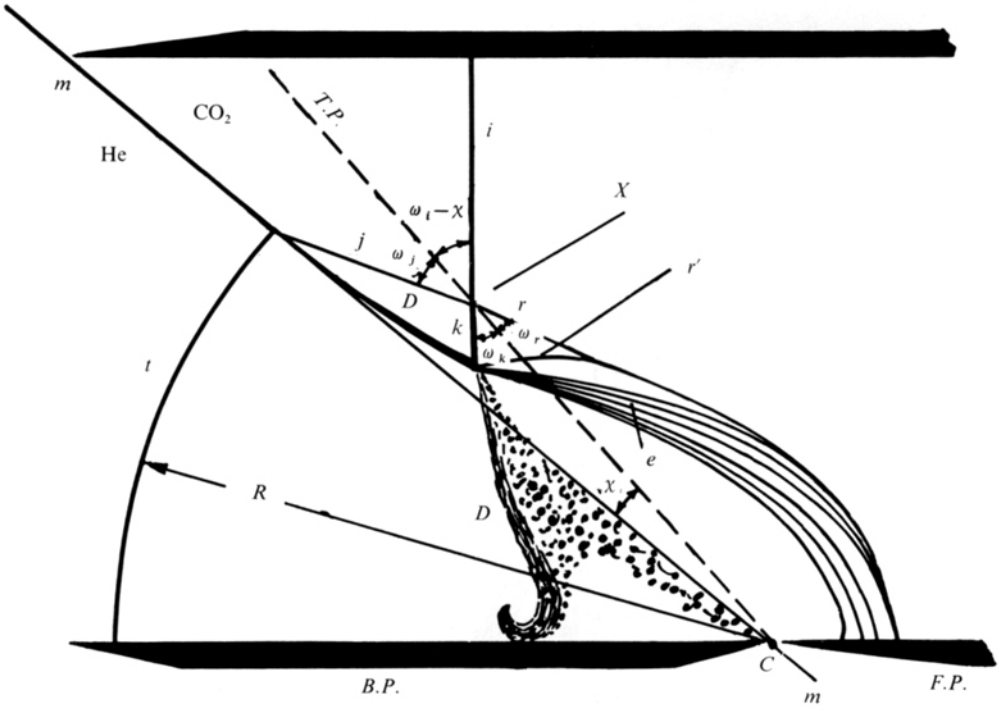

FIGURE 10. Free-precursor irregular refraction of a plane shock at a contaminated carbon dioxide–helium interface. *i*, incident shock; *t*, free-precursor transmitted shock (He); *j*, free-precursor shock (CO_2); *k*, modified incident shock; *r*, reflected shock; *r′*, weak shock reflected off the membrane; *e*, reflected expansion; *X*, shock interaction point; χ, trajectory angle of *X*; *T.P.*, trajectory path of *X*; *R*, radius; *C*, corner. For other symbols see caption to figure 3.

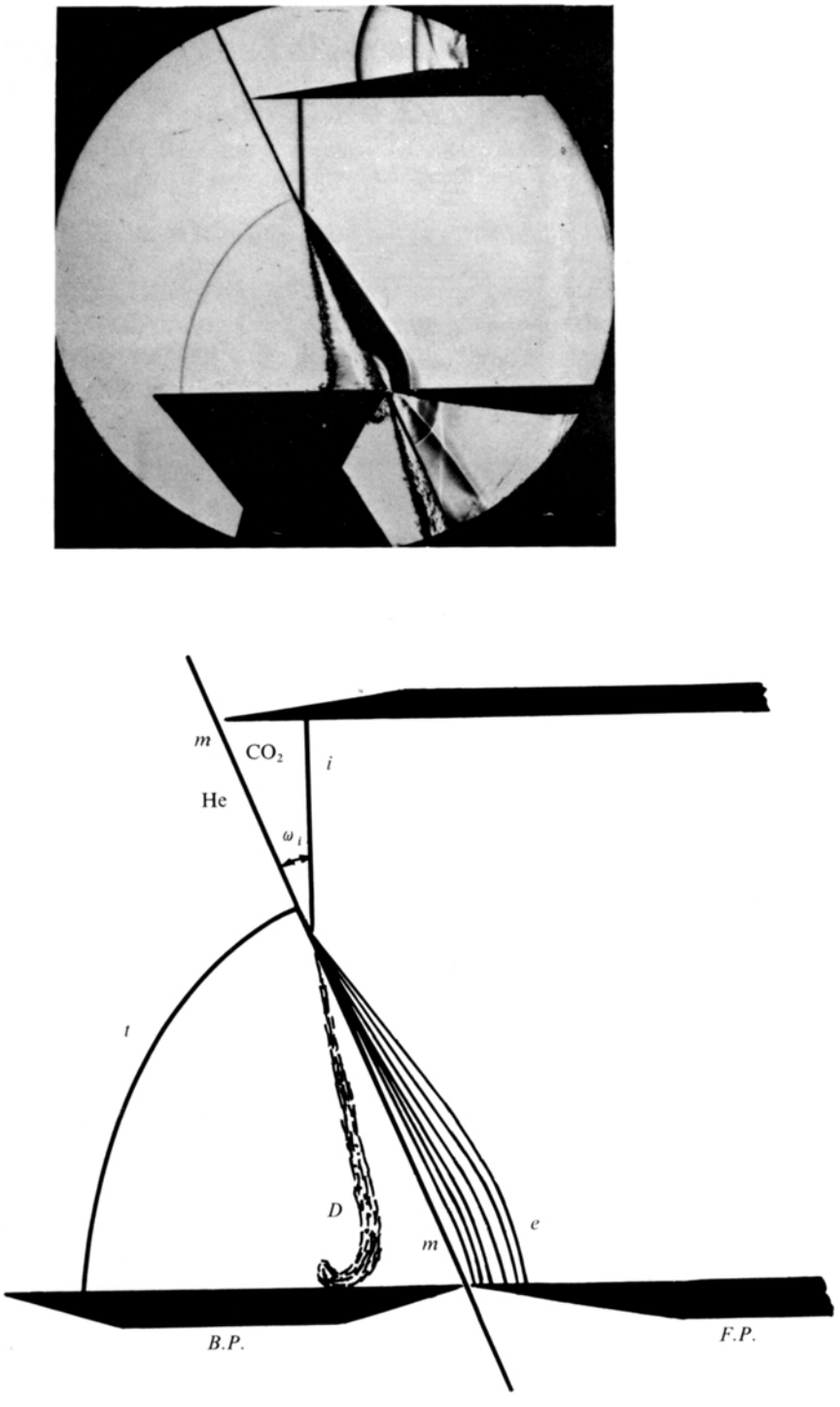

FIGURE 13. Bound-precursor irregular refraction of a plane shock at a contaminated carbon dioxide–helium interface. For symbols see captions to figures 3 and 10.